5866 *Chem. Mater.* **2010,** *22,* 5866–5875
DOI:10.1021/cm101745v

CHEMISTRY OF MATERIALS
Article

Transmission Electron Microscopy Study of $Ba_{0.5}Sr_{0.5}Co_{0.8}Fe_{0.2}O_{3-\delta}$ Perovskite Decomposition at Intermediate Temperatures

Konstantin Efimov,*,† Qiang Xu,‡,§ and Armin Feldhoff†

†*Institute of Physical Chemistry and Electrochemistry, Leibniz Universität Hannover, Callinstrasse 3-3a, 30167 Hannover, Germany,* ‡*National Centre for HREM, Kavli Institute of Nanoscience, Delft University of Technology, 2628 CJ Lorentzweg 1, Delft, The Netherlands, and* §*Vision Lab, University of Antwerp, 2020 Antwerp Groenenborgerlaan, 171, U316, Belgium*

Received June 22, 2010. Revised Manuscript Received September 9, 2010

The cubic perovskite $Ba_{0.5}Sr_{0.5}Co_{0.8}Fe_{0.2}O_{3-\delta}$ (denoted BSCF) is the state-of-the-art ceramic membrane material used for oxygen separation technologies above 1150 K. BSCF is a mixed oxygen-ion and electron conductor (MIEC) and exhibits one of the highest oxygen permeabilities reported so far for dense oxides. Additionally, it has excellent phase stability above 1150 K. In the intermediate temperature range (750−1100 K), however, BSCF suffers from a slow decomposition of the cubic perovskite into variants with hexagonal stacking that are barriers to oxygen transport. To elucidate details of the decomposition process, both sintered BSCF ceramic and powder were annealed for 180−240 h in ambient air at temperatures below 1123 K and analyzed by different transmission electron microscopy techniques. Aside from hexagonal perovskite $Ba_{0.6}Sr_{0.4}CoO_{3-\delta}$, the formation of lamellar noncubic phases was observed in the quenched samples. The structure of the lamellae with the previously unknown composition $Ba_{1-x}Sr_xCo_{2-y}Fe_yO_{5-\delta}$ was found to be related to the 15R hexagonal perovskite polytype. The valence and spin-state transition of cobalt leading to a considerable diminution of its ionic radius can be considered a reason for BSCF's inherent phase instability at intermediate temperatures.

Introduction

Cubic perovskite $Ba_{0.5}Sr_{0.5}Co_{0.8}Fe_{0.2}O_{3-\delta}$ (BSCF) is prominent in the family of mixed ionic and electronic conducting materials.[1,2] Owing to an exceptionally large amount of mobile oxygen defects in the highly symmetric perovskite lattice, BSCF exhibits very high oxygen-ionic transport rates over a wide temperature range.[3,4] Its extraordinary conducting properties combined with excellent phase stability at high temperatures make BSCF very promising for potential applications as semipermeable membranes in major processes like the separation of oxygen from air and the catalytic conversion of hydrocarbons.[5−8] Furthermore, the employment of BSCF as a cathode material in solid-oxide fuel cells (SOFCs) has also attracted a lot of attention.[9] In 2004, Shao and Haile reported the high power density of a symmetric single SOFC using BSCF as electrodes and a samaria-doped ceria (SDC) electrolyte at 773 and 873 K.[1] Since then, BSCF has been considered to be one of the most auspicious cathode materials for use in SOFCs operated in an intermediate temperature regime (IT-SOFC, T = 773−1073 K).[10]

Nevertheless, the wide applications of BSCF may be inhibited because of two major problems. First, the poor thermomechanical stability of the BSCF, namely low creep resistance and large coefficient of thermal expansion (CTE), can lead to the failure of the operation process in the worst case.[3,8,11] Second, the desired cubic structure of BSCF collapses at temperatures below 1123 K under long-term condition. In 2000, Shao et al. observed a slow decline of oxygen flux through a BSCF membrane after a long operation time at 1023 and 1098 K that was caused by an inherent phase transition.[4] A similar degradation of the oxygen permeation performance at 973 and 1023 K was also observed by van Veen et al. in 2003.[12] In order to elucidate this issue, Rebeilleau-Dassonneville et al. carried out an in situ X-ray diffraction (XRD) experiment and found the formation of noncubic phases in BSCF if the temperature was kept below 1073 K.[7] Moreover, Švarcová et al. investigated the long-term stability of BSCF at and below the crucial temperature of 1123 K by XRD.[13] Slow decomposition of the single cubic

*Corresponding author. E-mail: konstantin.efimov@pci.uni-hannover.de.

(1) Shao, Z.; Haile, S. M. *Nature* **2004**, *431*, 170.
(2) Chen, C.; Feng, S.; Ran, S.; Zhu, D.; Liu, W.; Bouwmeester, H. J. M. *Angew. Chem., Int. Ed.* **2003**, *115*, 5196.
(3) McIntosh, S.; Vente, J. F.; Haije, W. G.; Blank, D. H. A.; Bouwmeester, H. J. M. *Chem. Mater.* **2006**, *18*, 2187.
(4) Shao, Z.; Yang, W.; Cong, Y.; Dong, H.; Tong, J.; Xiong, G. *J. Membr. Sci.* **2000**, *172*, 177.
(5) Wang, H.; Cong, Y.; Xang, W. *Catal. Today* **2003**, *82*, 157.
(6) Caro, J.; Wang, H.; Tablet, C.; Kleinert, A.; Feldhoff, A.; Schiestel, T.; Kilgus, M.; Kölsch, P.; Werth, S. *Catal. Today* **2006**, *118*, 128.
(7) Rebeilleau-Dassonneville, M.; Rosini, S.; van Veen, A. C.; Farruseng, D.; Mirodatos, C. *Catal. Today* **2005**, *104*, 131.
(8) Vente, J. F.; Haije, W. G.; Rak, Z. S. *J. Membr. Sci.* **2006**, *177*, 2245.
(9) Shao, Z.; Haile, S. M.; Ahn, J.; Ronney, P. D.; Zhan, Z.; Barnett, S. A. *Nature* **2005**, *435*, 795.
(10) Zhou, W.; Ran, R.; Shao, Z. *J. Power Sources* **2009**, *192*, 231.
(11) Yi, J. X.; Lein, H. L.; Grande, T.; Yakovlev, S.; Bouwmeester, H. J. M. *Solid State Ionics* **2009**, *180*, 1564.
(12) van Veen, A. C.; Rebeilleau, M.; Farrusseng, D.; Mirodatos, C. *Chem. Commun.* **2003**, *1*, 32.
(13) Švarcová, S.; Wiik, K.; Tolchard, J.; Bouwmeester, H. J. M.; Grande, T. *Solid State Ionics* **2008**, *178*, 1787.

Published on Web 10/13/2010

perovskite phase into a 2H hexagonal polytype was detected in a BSCF powder that had been annealed for 24 h at 1023 K in ambient air. The phase transition process was observed to be much more pronounced after annealing of the BSCF samples for 240 h in flowing oxygen between 1073 and 1123 K. In this study, the hexagonal phase ratio expanded with decreasing temperature. The oxidation of the B-site cations (B = transitions metals), which leads to a change of effective ionic radii and gives the structure the Goldschmidt tolerance factor higher than one, was declared the reason for the inherent BSCF phase instability at intermediate temperatures.[13,14] In 2009, Arnold et al. reported the valence transition of cobalt in cubic BSCF from the predominantly 2+ state at 1223 K to the mixed 2+/3+ state at 298 K according to in situ electron energy loss spectroscopy (EELS).[15] Hence, they concluded that the oxidation of cobalt cations combined with their spin-state transition resulting in dramatic diminution of their ionic radius is the real driving force of the BSCF decomposition.[15]

Recently, Mueller et al. investigated the phase transition of cubic BSCF perovskite by combining XRD with transmission electron microscopy (TEM).[16] Their TEM micrograph of a BSCF ceramic that had been annealed for 8 days at 1073 K showed a grain boundary phase and lamellae that ran through the grains. The grain boundary phase was described as 2H−$Ba_{0.5+x}Sr_{0.5-x}CoO_{3-\delta}$ based on energy dispersive X-ray spectroscopy (EDXS) and selected area electron diffraction (SAED) along the *c*-axis. The latter is not sensitive to different stacking sequences, especially if they occur only at the very interface of the cubic phase, which can be expected accordingly to Arnold et al.[17] These lamellae were not addressed further. On the basis of their analysis, Mueller et al. proposed a simplistic phase diagram that put BSCF in a miscibility gap between the cubic and hexagonal phases, which were the only phases considered.[16]

Švarcová has suggested that the decomposition of BSCF might be reversible because annealed BSCF samples contain some of the same phases as the raw powder obtained after annealing for 240 h at 1023 K.[13] The relationship between the formation and decomposition processes of BSCF was also discussed by Arnold et al., who investigated the sol−gel synthesis of BSCF in detail.[17] XRD and high-resolution transmission electron microscopy (HRTEM) were applied to characterize crystalline intermediate phases in raw BSCF powder. A phase attribution of a sample quenched at 1023 K was provided in that report. Aside from the cubic (3C) and 2H hexagonal phases, the sample consisted of an additional phase of lower symmetry, which was described as a disordered hexagonal perovskite polymorph.

The findings of Arnold et al. offered inspiration to conduct a transmission electron microscopy (TEM) study of BSCF's decomposition process. For this reason, both sintered BSCF ceramic and powder were annealed for 180−240 h in ambient air at temperatures below 1123 K and extensively analyzed by several TEM techniques. Additionally, the functional properties of BSCF ceramic were tested by time-dependent oxygen permeation experiments under the aforementioned conditions.

Experimental Section

The BSCF powder was synthesized by a sol−gel route using ethylenediaminetetraacetic acid (EDTA) and citric acid as the organic ligand and network former, respectively. Given amounts of $Ba(NO_3)_2$, $Sr(NO_3)_2$, $Co(NO_3)_2$, and $Fe(NO_3)_3$ were dissolved in water, followed by the addition of EDTA and citric acid. The pH value of the solution was adjusted to the range of 7−9 with $NH_3 \cdot H_2O$. The transparent reaction solution was then heated at 423 K under constant stirring for several hours until a purple-colored gel was obtained. The gel was then precalcined in the temperature range of 573−673 K. Following, the precalcined powders were ground and fired at 1223 K for 10 h. To obtain the BSCF ceramic, the powder was uniaxially pressed under 140−150 kN for 20 min into green bodies. The pellets were then calcined for 10 h at 1423 K with a heating and cooling rate of 3 K/min.

An oxygen permeation measurement was performed on a dense membrane disk with a diameter of 16 mm and a thickness of 1.1 mm in a high-temperature permeation cell according to the method described elsewhere.[18,19] The reactor temperature was kept constant at 1023 K for more than 240 h. Air was fed at a rate of 150 mL min^{-1} to the feed side; He (29.0 mL min^{-1}, 99.995%) and Ne (1.0 mL min^{-1}, 99.995%), which were used to determine the absolute flux rate of the effluents, were fed to the sweep side. The effluents were analyzed by gas chromatography on an Agilent 6890 instrument equipped with a Carboxen 1000 column. Gas concentrations in the effluent stream were calculated from a gas chromatograph calibration.

A powder XRD sample was obtained from the BSCF ceramic after annealing at 1023 K for 240 h and subsequent grinding. The XRD data were collected in a $\Theta/2\Theta$ geometry on a Philips X'pert-MPD instrument with monochromated Cu Kα radiation at 40 kV and 40 mA and a receiving slit of 0.05 mm using a step−scan mode in the 2Θ range of 15°−90° with intervals of 0.02°.

In order to obtain a TEM sample, the annealed BSCF ceramic was cut into rectangular pieces of 1 mm × 1.5 mm × 3 mm. The BSCF powder sample was epoxy glued between two pieces of silicon wafer before cutting. Subsequently, the pieces were polished on polymer-embedded diamond lapping films to approximately 0.01 mm × 1 × 2.5 mm (Allied High Tech, Multiprep). Finally, Ar^+ ion sputtering was employed at 3 kV (Gatan, model 691 PIPS, precision ion polishing system) under shallow incident angles in the range of 4−8° until electron transparency was achieved.

Scanning TEM (STEM) and TEM, as well as SAED, were conducted at 200 kV on a JEOL JEM-2100F-UHR field-emission instrument equipped with an ultrahigh-resolution pole piece that provided a point-resolution better than 0.19 nm (spherical

(14) Goldschmidt, V. M. *Naturwissenschaften* **1926**, *14*, 477.
(15) Arnold, M.; Xu, Q.; Tichelaar, F. D.; Feldhoff, A. *Chem. Mater.* **2009**, *21*, 635.
(16) Mueller, D. N.; De Souza, R. A.; Weirich, T. E.; Roehrens, D; Mayer, J.; Martin, M. *Phys. Chem. Chem. Phys.* **2010**, *12*, 10320.
(17) Arnold, M.; Gesing, T. M.; Martynczuk, J.; Feldhoff, A. *Chem. Mater.* **2008**, *20*, 5881.
(18) Wang, H.; Tablet, C.; Feldhoff, A.; Caro, J. *J. Membr. Sci.* **2005**, *262*, 20.
(19) Martynczuk, J.; Arnold, M.; Feldhoff, A. *J. Membr. Sci.* **2008**, *322*, 375.

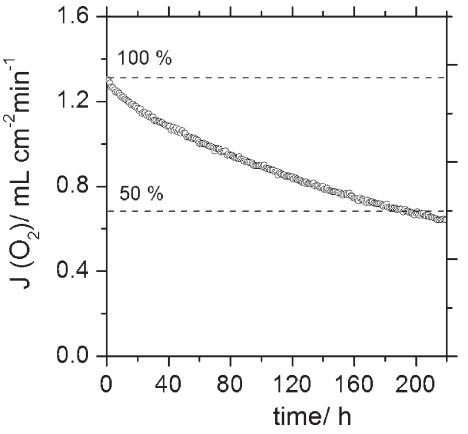

Figure 1. Oxygen permeation flux through BSCF membrane as a function of time at 1023 K.

aberration constant $C_S = 0.5$ mm; chromatic aberration constant $C_C = 1.2$ mm) and allowed high-resolution TEM (HRTEM) acquisition. A light element EDX spectrometer, Oxford Instruments INCA-200 TEM, was used for elemental analysis. An energy filter of the type Gatan GIF 2001 was employed to acquire electron energy-loss spectra (EELS). HR-STEM high angle annular dark field (HAADF) experiments were conducted with an FEI Titan electron microscope equipped with an aberration image corrector at 300 kV

Results and Discussion

The oxygen permeation performance of the BSCF ceramic was tested at 1023 K. As demonstrated in Figure 1, the oxygen flux through the BSCF membrane decayed continuously to about 50% after 240 h. This result was in good agreement with the results reported by Shao et al.[4] and van Veen et al.[12] The degradation of the BSCF functional properties at intermediate temperatures can be due to several reasons. First, the concentration of mobile oxygen vacancies in the perovskite lattice can be decreased due to a change in oxidation state of the B-cations, as recently reported.[12,20] Second, the continuously decreasing oxygen permeation performance of BSCF under long-term conditions can be explained by the growth of noncubic phases during operation, which might act as barriers, and by a change of stoichiometry of the cubic phase.

Figure 2a,b shows the XRD data taken from the BSCF powder as well as from ground BSCF ceramic after annealing at 1073 K for 180 h and at 1023 K for 240 h, respectively. Obviously, the cubic perovskite remained as the major phase in both samples. However, the presence of noncubic phases was evident on the basis of the weak additional intensities between 25° and 28° and 42.5° 2Θ, which are marked with an asterisk. Rebeilleau-Dassonneville et al. observed additional reflections at the same positions in the BSCF diffraction pattern during in situ XRD experiments at temperatures below 1023 K.[7] Thus, it may be concluded that the noncubic phases arose before quenching of the sample. Due to the restricted number of reflections from the noncubic phases and those weak intensities, the

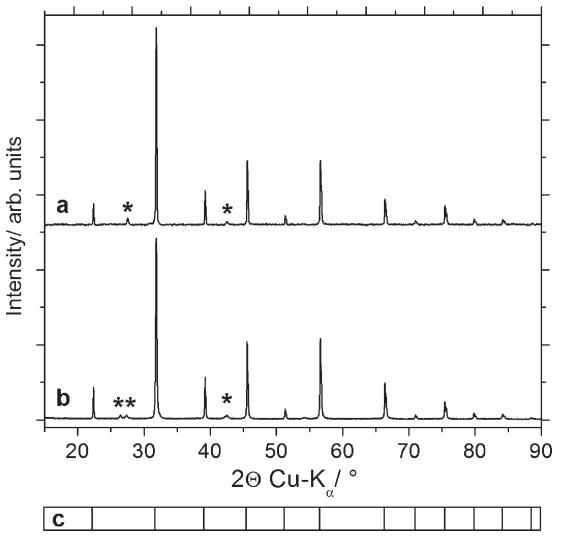

Figure 2. (a) XRD pattern of the BSCF powder after annealing at 1073 K for 180 h. (b) XRD pattern of the BSCF ceramic after annealing at 1023 K for 240 h. The intensities corresponding to noncubic phases are marked with asterisks. (c) The Bragg positions correspond to cubic perovskite with $a = 0.398$ nm.

noncubic phases could not be identified by XRD in this work either.

Nevertheless, with help of several TEM methods, it was possible to detect and analyze the noncubic phases in the annealed BSCF powder and ceramic samples. A TEM dark-field micrograph in Figure 3a shows an area of the powder sample. An interface between two grains is clear in this image. A HRTEM (Figure 3b) micrograph of the marked grain showed a hexagonal symmetry of the grain structure. Furthermore, the fast Fourier transform (FFT) in Figure 3c can be explained by the reciprocal lattice of hexagonal perovskite being viewed along the $[0,1,0]_{hex}$ orientation due to a spacing of 0.49 nm between the $(100)_h$ planes and $(010)_h$ planes. The chemical composition of the hexagonal phase was determined by EDX spectroscopy to be $Ba_{0.6}Sr_{0.4}CoO_{3-\delta}$. Hexagonal perovskites with similar composition have been previously reported by Gushee et al.[21] and Taguchi et al.[22] Accordingly, the transition of cubic BSCF into a hexagonal perovskite phase after annealing at intermediate temperatures, as reported by Švarcová et al.[13] and Mueller et al.,[16] was confirmed during the current TEM study.

Furthermore, the partial transformation of cubic BSCF to noncubic phases, which had the shape of lamellae, was observed in the treated powder sample. Similar lamellae could be seen in the TEM micrograph of Mueller et al., but they were not addressed further there.[16] A HRTEM micrograph in Figure 4a shows one lamella and the parent phases. The structure of the lamella, which was approximately 50 nm wide, consisted mainly of periodically ordered segments with a distance of 1.19 nm between them. As can be observed in the SAED pattern of the corresponding sample area in Figure 4b, which was acquired from the

(20) Kriegel, R; Kircheisen, R; Töpfer, J. *Solid State Ionics* **2010**, *181*, 64.

(21) Gushee, B. E.; Katz, L.; Ward, R. *J. Am. Ceram. Soc.* **1957**, *79*, 5601.

(22) Taguchi, H.; Takeda, Y.; Kanamaru, F.; Shimada, M.; Koizumi, M. *Acta Crystallogr., Sect. B* **1977**, *33*, 1299.

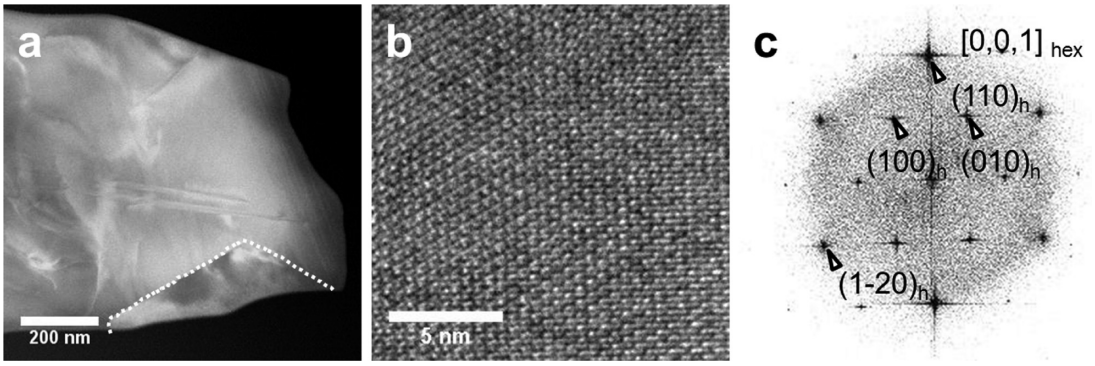

Figure 3. (a) STEM annular dark-field micrograph showing an interface between two grains in the BSCF powder sample annealed at 1073 K for 180 h. (b) HRTEM micrograph of the marked grain. (c) Power spectrum of (b).

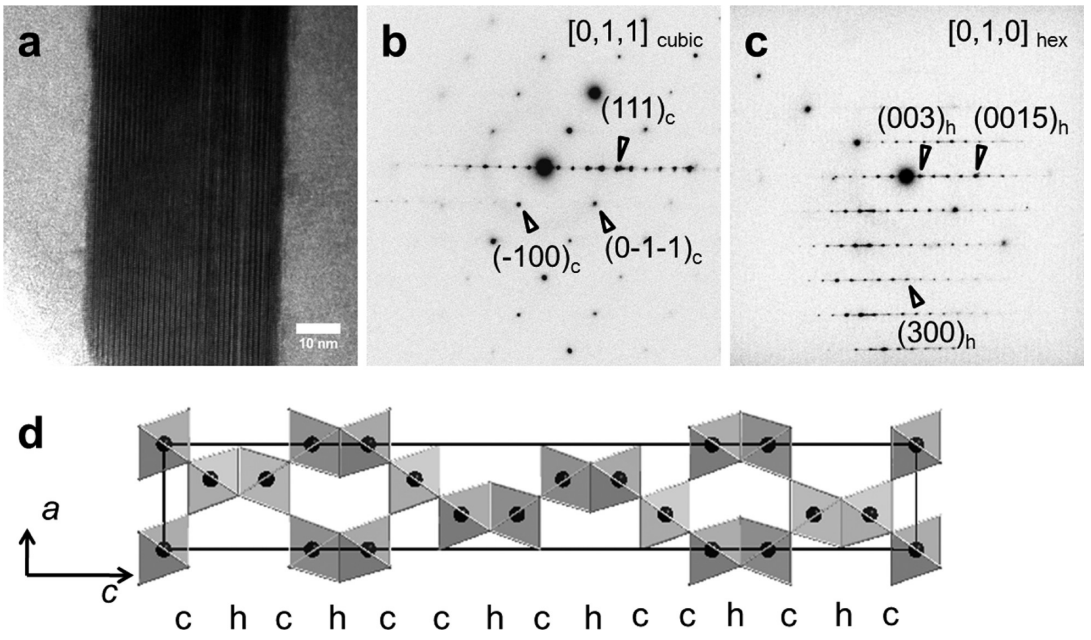

Figure 4. (a) HRTEM micrograph showing a lamella in the BSCF powder sample after annealing at 1073 K for 180 h. (b) SAED pattern from the corresponding area. (c) SAED pattern from the lamella achieved by tilting of the sample. (d) 15R structural model viewed along the [0,1,0] direction using $(cchch)_3$ stacking sequences of BO_6 octahedra.

selected sample area with a size of approximately 260 nm, the lamella grew in the cubic perovskite grain oriented along the $[0,1,1]_{cubic}$ direction. The segments of the lamella were arranged parallel to the $(111)_{cubic}$ plane. The spacing between the lamella segments was approximately equal to a 5-fold (111) spacing of cubic perovskite ($d_{(111)} = 0.23$ nm), which corresponds to the spacing between cubic-close packed AO_3 layers. Hence, it can be concluded that one segment of the lamella consisted of five close-packed layers. Note that these five close-packed layers were not necessarily all cubic-close stacked. Some of them may have been hexagonal-close stacked, making the whole structure a noncubic phase. Similar structures containing five-layered segments were once described for hexagonal perovskite polytypes of 5H $BaCoO_{3-\delta}$ by Miranda et al., as well as 15R $SrMn_{1-x}Fe_xO_{3-\delta}$ by Cussen et al.[23,24] The SAED pattern from the lamella shown in Figure 4c was obtained by tilting of the sample. The intensity distribution of the diffraction data revealed the rhombohedral symmetry of the lamella, which can be explained using a hexagonal unit cell. The rhombohedral symmetry of the lamella structure appeared if the close-packed layers were arranged in a $(cchch)_3$ stacking sequence along the c_{hex} axis, as shown in the Figure 4d. Moreover, the lamella's diffraction pattern exhibited a distinct correlation with the diffraction pattern of 15R $SrMn_{1-x}Fe_xO_{3-\delta}$ with the $(cchch)_3$ stacking sequence viewed along the $[0,1,0]_{hex}$ direction.[24] Consequently, the lamella can be considered a 15R related phase with a hexagonal unit cell. The lattice parameter $c_{hex} \approx 3.57$ nm of the unit cell was estimated from the HRTEM and SAED. The parameter $a_{hex} \approx 0.56$ nm was estimated using the formula $a_{hex} = a_{cubic}((2)^{1/2})$.[25] The relationship between cubic perovskite and hexagonal perovskite polytypes in terms of the cubic-closed and

(23) Miranda, L.; Feteira, A.; Sinclair, D. C.; Hernández, M. G.; Boulahya, K.; Hernando, M.; Varela, A.; González-Calbet, J. M.; Parras, M. *Chem. Mater.* **2008**, *20*, 2818.
(24) Cussen, E. J.; Sloan, J.; Vente, J. F.; Battle, P. D.; Gibb, T. C. *Inorg. Chem.* **1998**, *37*, 6071.
(25) Mitchell, R. H. *Perovskites: Modern and Ancient*; Almaz Press Inc.: Ontario, Canada, 2002.

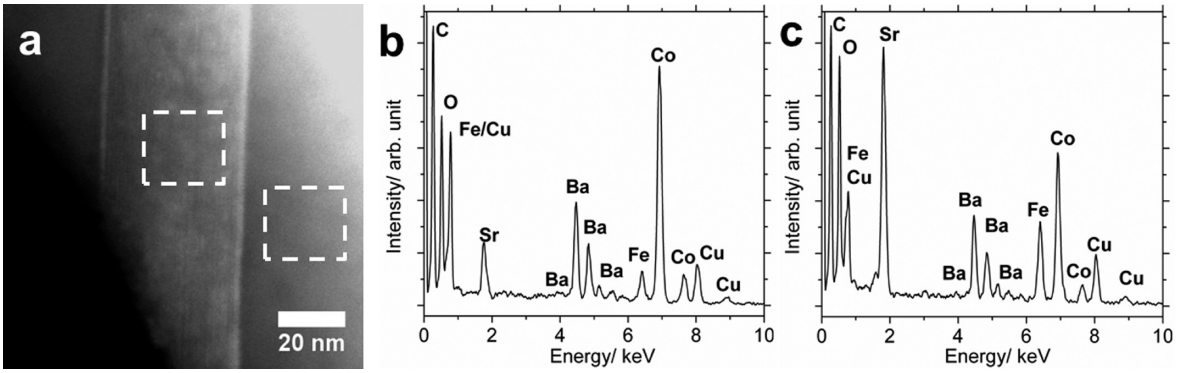

Figure 5. (a) STEM annular dark-field micrograph with labeling of scanned areas for elemental analysis. (b) EDX spectrum of the lamella. (c) EDX spectrum of the parent cubic phase. C and Cu lines appear due to a narrow TEM pole piece.

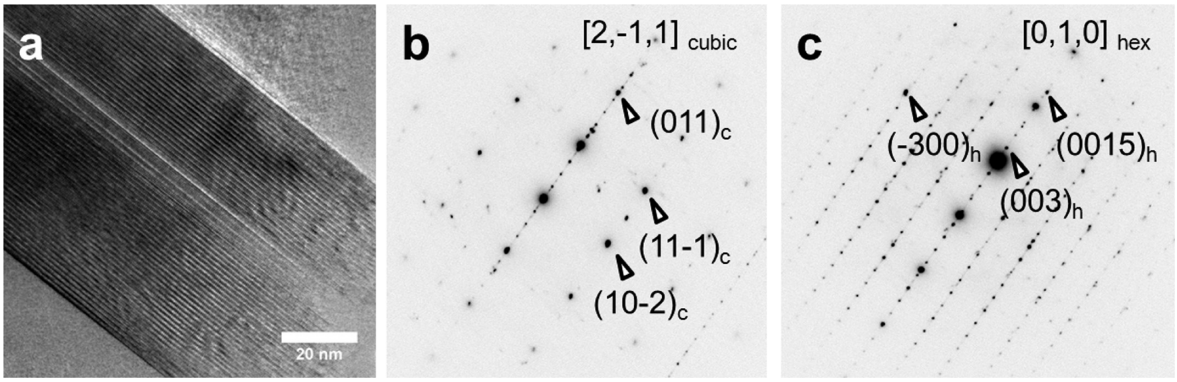

Figure 6. (a) HRTEM micrograph showing the lamella in the BSCF ceramic sample annealed at 1023 K for 240 h. (b) SAED pattern from the lamella and the matrix. (c) SAED pattern from the lamella achieved by tilting of the sample as compared to (b).

hexagonal-closed stacking of AO_3 was described by Katz et al. in detail.[26] A possible pathway of the transition from cubic perovskite to hexagonal polymorphs via a shear of the AO_3 layers has been reported by Arnold et al.[15,27] In terms of the cubic cell, the AO_3 layers oriented perpendicular to the [1,1,1] cubic zone axis form cubic-close packing. B-cations occupy the octahedral holes, and octahedra generate a three-dimensional corner-sharing array. The shear of some AO_3 layers leads to the formation of hexagonal-close packing and face-shared octahedral columns along the [1,1,1] cubic orientation. The arrangement of the five-layered sequences of the lamella parallel to the (111) cubic plane can be explained with this pathway.

By STEM high angle annular dark-field (HAADF) and EDXS experiments, anomalies of the lamellar chemical composition could be observed. The STEM HAADF micrograph in Figure 5a shows inhomogeneous elemental distribution inside of the lamella in spots with a bright Z-contrast. Figure 5b shows an EDX spectrum acquired from a wide area of lamella labeled in Figure 5a. Using Cliff-Lorimer quantification, a considerable accumulation of cobalt of up to 63 atom % of the total value of cations was detected in the lamella. A moderate enrichment of barium of up to 30 atom % as well as a strong depletion of strontium and iron was also observed. On average, the amount of the B-cations exceeded the content of A-cations in the lamella by 2-fold. Thus, the EDX spectroscopy delivered surprising results, because hexagonal perovskite-related phases with such stoichiometry are not known. In contrast, the spectrum of the matrix phase (Figure 5c) showed the expected intensity distribution of element lines for the cubic BSCF perovskite.

Lamellar phases were also found in the BSCF ceramic sample annealed at 1023 K for 240 h. One of them is displayed in the HRTEM micrograph in Figure 6a. The lamella were mainly organized in periodically stacked segments. Furthermore, in the middle of the lamella, a thin area with a nonperiodic arrangement of the segments was observed. The SAED pattern from the lamella and the matrix acquired from the selected sample area with a size of approximately 260 nm (Figure 6b) revealed that the lamellae grew in the cubic perovskite grain oriented along the $[2,\bar{1},1]_{cubic}$ zone axis. The segments of the lamella were arranged parallel to the (011) cubic plane. The spacing between periodic segments was 1.19 nm, which is the same distance between segments of the lamella found in the powder sample. By tilting of the sample, the lamella were oriented along the $[0,1,0]_{hex}$ direction. The intensity distribution in the SAED pattern in Figure 6c shows rhombohedral symmetry of the lamellar structure. The comparison of the diffraction data from the lamella in the ceramic sample with the SAED pattern from the

(26) Katz, L.; Ward, R. *Inorg. Chem.* **1964**, *3*, 205.
(27) Arnold, M.; Wang, H.; Martynczuk, J.; Feldhoff, A. *J. Am. Ceram. Soc.* **2007**, *90*, 3651.

lamella in the powder sample (Figure 4c) lead to the conclusion that the lamellae were isostructural with each other. However, the lamella formed in the annealed ceramic did not grow parallel to the close-packed layer of the cubic matrix; the regular part of the lamella can instead be explained by a 15R-related structure. Diffraction spots that cannot be attributed to the 15R setting are likely related to the stacking faults in the middle area of the lamella in Figure 6a.

EDX spectroscopy investigations of the chemical composition indicated the presence of twice the amount of B-cations compared to A-cations in the lamella in the ceramic sample. In order to elucidate structural information in accordance with the chemical composition of the lamellae, which is unusual for hexagonal perovskite-related compounds, high resolution (HR) STEM HAADF experiments were carried out that determine the positions of atoms by mass-density contrast distribution. The HR-STEM HAADF micrograph in Figure 7a and Fourier averaged HRSTEM micrograph in Figure 7b show further lamella in the annealed ceramic sample. The lamella is viewed along the $[\bar{1},1,0]_{hex}$ direction. In this projection, it is clearly evident that the regular segments of the lamella structure contain five layers: three layers consisting of bright dots and two dark rows separated by chains with lower contrast in between. The dots with a bright Z-contrast relate to the positions of A-cations due to their atomic weight, and the two dark rows indicate missing A-cation positions. The Z-contrast intensity distribution of the layers achieved from the marked area in the Fourier averaged STEM micrograph is plotted in Figure 7c. The average contrast ratio between the chain with medium contrast and three layers with bright contrast was 0.67. According to the relationship of the lamella structure to the 15R setting and the results of EDX spectroscopy, the three layers with bright contrast in Figure 7a,b relate to columns containing A-cations (mostly barium) and oxygen. The chain with medium contrast corresponds to double B-cation (mostly cobalt) columns. The contrast ratio between the columns was calculated as follows: ratio = $Z(Co + Co)^2/Z(Ba + O)^2 = 0.71$, which is consistent with the measured contrast ratio. As suggested by the Z-contrast pattern and intensity distribution, a structural model of the five-layered segment of the regular part of the lamella viewed along the $[\bar{1},1,0]$ orientation, as shown in Figure 7d, was proposed. The lamella structure is assembled from three AO_3 layers and two O_3 layers, which are in a quasi-close-packed arrangement along the c_{hex} axis. B-cations occupy a quarter of the octahedral sites between the layers, as in the perovskite structure. Additionally, a quarter of the disordered octahedral sites between the two O_3 layers is occupied by extra B-cations. In the structural model, the circles point to columns with A-cation vacancies and the arrows mark the double B-cation columns. The chemical composition of the lamella can be described with the general formula of $(A_3B_6O_{15})_3$, corresponding to the 15R setting. According to results of EDX spectroscopy and HRSTEM, as well as the expected presence of oxygen vacancies, an empirical formula of $Ba_{1-x}Sr_xCo_{2-y}Fe_yO_{5-\delta}$ of the lamella phase is proposed. The report from Sun et al. concerning new barium cobaltite $Ba_3Co_{10}O_{17}$ gives a further insight into the development of a $Ba_{1-x}Sr_xCo_{2-y}Fe_yO_{5-\delta}$ structure model, because $Ba_3Co_{10}O_{17}$ exhibits the 15R related structure containing close-packed BaO_3 and an oxygen layer array with completely occupied octahedral sites with cobalt cations in the oxygen layer.[28]

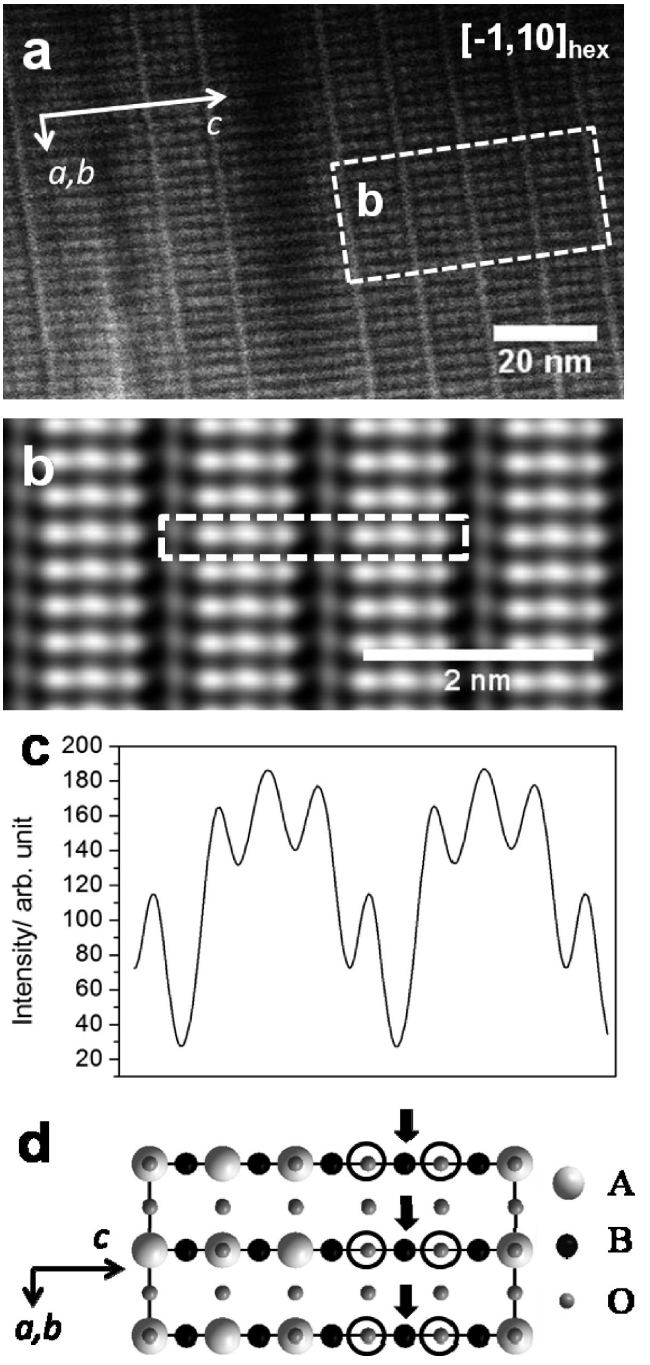

Figure 7. (a) HR-STEM annular dark-field micrograph of the lamella viewed along the $[\bar{1},1,0]_{hex}$ direction. (b) Fourier averaged HR-STEM micrograph from the area labeled in (a). (c) Z-contrast intensity distribution taken from the area labeled in (b). (d) Schematic representation of the five-layered segment of the $Ba_{1-x}Sr_xCo_{2-y}Fe_yO_{5-\delta}$ structure as suggested by the Z-contrast pattern. Circles mark A-cation vacancies, and arrows point to double B-cations columns.

(28) Sun, J.; Yang, M.; Li, G.; Yang, T.; Liao, F.; Wang, Y.; Xiong, M.; Lin, J. *Inorg. Chem.* **2006**, *45*, 9151.

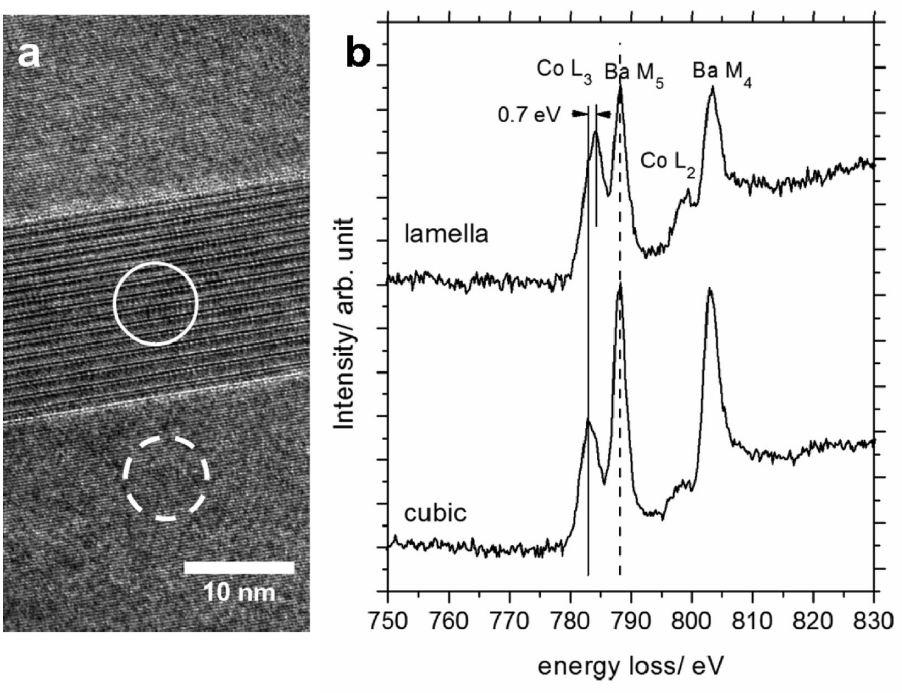

Figure 8. (a) HRTEM micrograph with labeling of area for EELS. (b) Electron energy-loss spectra showing cobalt-$L_{2,3}$ and barium-$M_{4,5}$ ionization edges of lamella and the cubic phase.

Furthermore, with the help of the HR-STEM HAADF micrograph in the Figure 7a, the above-mentioned inhomogeneous elemental distribution in the lamellae can be explained. Obviously, in some areas of the lamella, all barium sites in the close-packed layer remained occupied.

The significant difference between phases with hexagonal stacking of close-packed layers from the cubic perovskites is the up to 10 pm closer B-site cation−oxygen distances in the octahedral sites. Accordingly, smaller cations favor occupation at the octahedral sites in the hexagonal stacking. The ionic radius of multivalent B-cations is strongly connected with their valence and spin state.[29] Because the structure of the lamellae contains hexagonal-close packed layers, an average higher valence of B-cations, especially cobalt, compared to cubic perovskite is expected. In order to verify this assumption, EEL spectra were acquired from the cubic phase and $Ba_{1-x}Sr_xCo_{2-y}Fe_yO_{5-\delta}$ lamella of the ceramic sample annealed at 1023 K for 240 h corresponding to the marked areas in a Figure 8a. The cobalt $L_{2,3}$ and barium $M_{4,5}$-edges from the cubic phase and lamella are plotted in the Figure 8b. The EEL spectrum of the lamella showed a significant increase in the cobalt-L_3/barium-M_5 and cobalt-L_2/barium-M_4 intensity ratios as compared to the spectra from the cubic phase. This fact confirms the accumulation of cobalt in the lamella. An additional feature of the EEL spectra from the lamella was the shift of the cobalt L_3-edge position at approximately 0.7 eV to a higher energy loss, which was determined using the barium M_5-edge (788 eV at maximum) as an internal standard.[15] A reason for the L_3-edge shift is the increase in the average cobalt valence in the lamellae.[30] Arnold et al. determined the mixed 2+/3+ valence state of cobalt with absolute value of 2.6+ in the cubic BSCF perovskite at room temperature by comparing the cobalt L_3-edge of cubic BSCF with those of well-known materials.[26] However, the measured value of cobalt valence may be slightly higher due to the long-term annealing at intermediate temperatures, as reported by Kriegel et al.[16] In comparison, the valence state of cobalt in the $Ba_{1-x}Sr_xCo_{2-y}Fe_yO_{5-\delta}$ lamella was close to +3 and was measured in the same way that the shift of the cobalt L_3-edge was monitored. Then, the predominantly valence state of cobalt of 3+ in the lamella phase can be estimated. The presence of a certain amount of Co^{4+} in the lamella phase is expected also.[31] As a consequence of the rising valence of cobalt, the amount of oxygen vacancies (δ) in the lamella should be considerably lower than that in the cubic matrix. Combined with the low crystal symmetry, the presence of lamellae in BSCF can be considered to be unfavorable for its oxygen conducting properties. Because lamellae are several micrometers long, they can be considered as barriers to ionic oxygen transport through a BSCF membrane.

The findings of the EELS experiments confirmed the driving force of the BSCF decomposition postulated by Arnold et al.,[15] who suggested that it was a temperature-dependent change of cobalt valence coupled with a partial spin-state transition of cobalt ions.[31,32] The oxidation of cobalt leads to a diminution of its ionic radius from Co^{2+}-(high spin) = 74.5 pm to Co^{3+}(high spin) = 61 pm, Co^{3+}-(low spin) = 54.5 pm, and Co^{4+}(high spin) = 53 pm.[29] The

(29) Shannon, R. D. *Acta Crystallogr., Sect. A* **1976**, *32*, 751.
(30) Yoon, W. S.; Kim, K. B.; Kim, M. G.; Lee, M. K.; Shin, H. J.; Lee, J. M.; Lee, J. S. *J. Phys. Chem. B* **2002**, *106*, 2526.
(31) Harvey, A. S.; Yáng, Z.; Infortuna, A.; Beckel, D.; Purton, J. A.; Gauckler, L. J. *J. Phys.: Condens. Matter* **2009**, *21*, 015801.
(32) Harvey, A. S.; Litterst, F. J.; Yáng, Z.; Rupp, J. L. M.; Infortuna, A.; Gauckler, L. J. *Phys. Chem. Chem. Phys.* **2009**, *11*, 3090.

small cobalt cations are not tolerated in the cubic perovskite structure because they favor occupying the face-shared octahedral sites in the hexagonal stacking with a closer B−O distance. The observation of Nagai et al. suggests a labile cobalt valence and spin state as being responsible for BSCF decomposition, because many cobalt-based cubic perovskites break down via the formation of hexagonal/cubic phase mixtures at temperatures below 1173 K.[33] Furthermore, the cobalt-free iron-based cubic perovskites of the compositions $(Ba_{0.5}Sr_{0.5})(Fe_{0.8}Cu_{0.2})O_{3-\delta}$ and $(Ba_{0.5}Sr_{0.5})(Fe_{0.8}Zn_{0.2})O_{3-\delta}$, which are related to BSCF, show good stability under long-term conditions at temperatures below 1173 K, owing to the less flexible redox behavior of iron.[34−36]

We observed about 20 sample areas in both the BSCF powder annealed at 1073 K for 180 h and the sintered ceramic annealed at 1023 K for 240 h. We observed that the growth of lamellae often occurred in various directions in the cubic perovskite grain. Such a situation is obvious in the TEM bright field micrograph in Figure 9a, which shows several micrometer-long lamellae arranged in three different directions in the ceramic sample. The matrix phase was characterized by the HRTEM micrograph in Figure 9b combined with the two-dimensional fast Fourier transformation (FFT) from the corresponding area (Figure 9c) to be a cubic perovskite grain, viewed along the $[0,1,1]_{cubic}$ zone axis. Note that the lamellae grew through the BSCF grain bulk and not along the grain boundaries. The lamellae marked in Figure 9a with a dashed line are also shown in Figure 9b under high resolution magnification. The FFT from the related area in Figure 9d exhibited a reciprocal lattice of the $Ba_{1-x}Sr_x$-$Co_{2-y}Fe_yO_{5-\delta}$ structure viewed along the $[\bar{1},1,0]_{hex}$ orientation. The segments of the lamella formed parallel to the (100) cubic plane. The lamella marked in Figure 9a with the dotted line were located at an angle of approximately 25°. Because the angle between the (100) and $(3\bar{1}1)$ cubic planes amounted to 25.24°, the growth direction of the lamella was indicated to be parallel to the $(3\bar{1}1)$ cubic plane. The growth direction of the lamella marked with the dashed-dotted line parallel to the $(2,\bar{1},1)$ cubic direction was determined analogously to the angle between the lamellae of approximately 35° and the angle between the (100) and $(2,\bar{1},1)$ cubic directions of 35.26°. The formation of lamellae along the (100), $(2\bar{1}1)$, and $(3\bar{1}1)$ cubic directions cannot be explained by the shear of close-packed layers of the cubic parent phase. A geometrical approach considering tilting of the coordination polyhedrons does not provide a solution either. It appears that complex reconstructive transformations influenced by the change of chemical composition occurred during the BSCF decomposition process. Recently, Yi et al. attested high creep rates of BSCF at the relevant temperatures. The creep was found to be controlled by cation diffusion.[11] Hence, the high cation mobility in the BSCF delivers a possible explanation for the BSCF phase transition into compounds with unusual compositions via complex pathways.

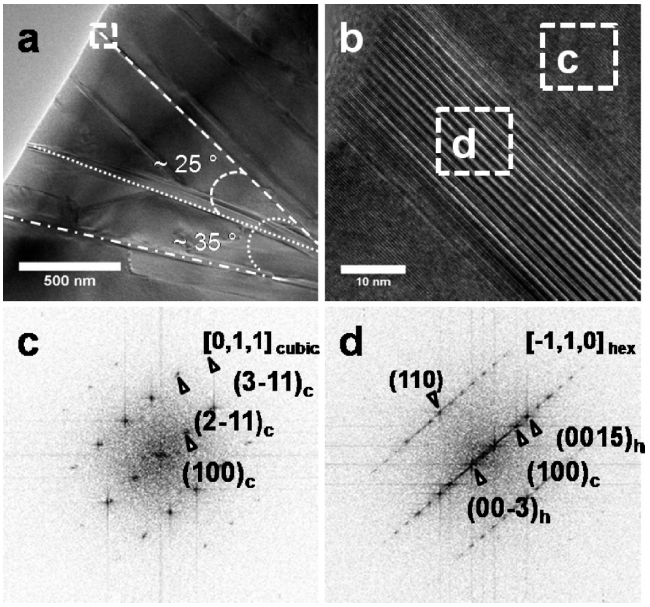

Figure 9. (a) TEM bright-field micrograph of the annealed BSCF ceramic sample showing lamellae grown along different directions. (b) HRTEM micrograph of the marked area in (a). (c, d) Two-dimensional fast Fourier transformed related to the marked areas in (b).

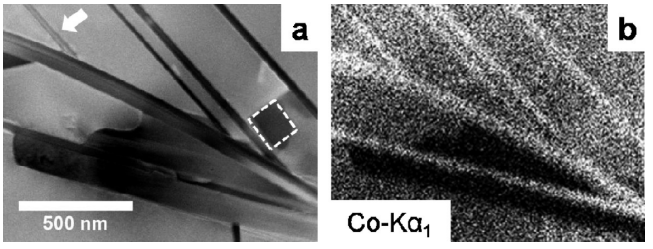

Figure 10. (a) STEM annular dark-field micrograph showing platelike phases adjacent to lamellae. Arrow marks the lamella shown in Figure 11. Rectangle marks the area of the $Ba_{0.6}Sr_{0.4}CoO_{3-\delta}$ composition. (b) Cobalt distribution by EDX spectroscopy using the Co $K\alpha_1$ line.

Due to the fact that the lamellae are cobalt enriched, the presence of phases with low cobalt concentrations were expected in the annealed BSCF samples. Indeed, cobalt-depleted phases were detected by EDXS. Figure 10a shows the STEM HAADF micrograph that was acquired from the detail of the sample area presented in Figure 9a showing platelike phases adjacent to the lamellae. In the elemental distribution by EDXS in Figure 10b, a strong depletion of cobalt in the platelike phases is clearly evident. Furthermore, the Cliff-Lorimer quantification of the EDXS data indicated a slight accumulation of strontium of up to 60 atom % of the total value of cations, as well as an absence of iron in these phases. According to the EDXS results, the platelike phases are related to a mixed barium strontium oxide with the stoichiometry $Ba_{0.4}Sr_{0.6}O$. With help of EDX spectroscopy, a phase was detected (marked by a rectangle in the STEM HAADF

(33) Nagai, T.; Ito, W.; Sakon, T. *Solid State Ionics* **2007**, *177*, 3433.
(34) Efimov, K.; Halfer, T.; Kuhn, A.; Heitjans, P.; Caro, J.; Feldhoff, A. *Chem. Mater.* **2010**, *22*, 1540.
(35) Martynczuk, J.; Efimov, K.; Robben, L.; Feldhoff, A. *J. Membr. Sci.* **2009**, *344*, 62.
(36) Feldhoff, A.; Martynczuk, J.; Arnold, M.; Myndyk, M.; Bergmann, I.; Šepelák, V.; Gruner, W.; Vogt, U.; Hähnel, A.; Woltersdorf, J. *J. Solid State Chem.* **2009**, *182*, 2961.

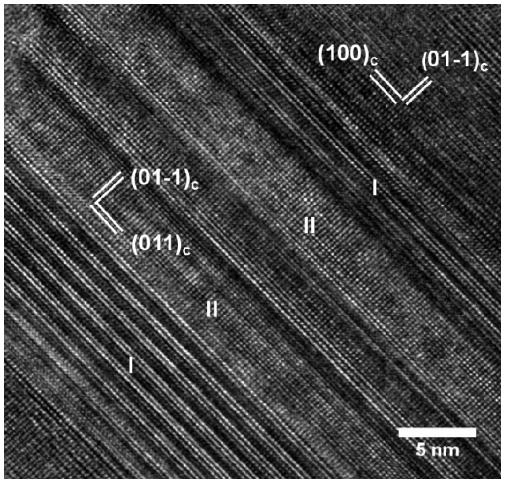

Figure 11. HRTEM micrograph showing the presence of cubic phase inside the lamella.

micrograph in Figure 10a) that contained barium, strontium, and cobalt in proportions similar to the hexagonal perovskite $Ba_{0.6}Sr_{0.4}CoO_{3-\delta}$. Further, a lower amount of cobalt in one lamella marked by an arrow in Figure 10a compared to other lamellae was found by quantification of the EDXS data. This lamella is shown in the HRTEM micrograph in Figure 11. Obviously, the lamella contained areas with different structures. The areas "I" on the edges of the lamella exhibited the 15R-related $Ba_{1-x}Sr_xCo_{2-y}Fe_yO_{5-\delta}$ structure viewed along the $[\bar{1},1,0]_{hex}$ orientation. The areas "II" in the middle of the lamella had a cubic structure and are viewed along the $[1,0,0]_{cubic}$ zone axis, different from the parent cubic phase oriented along the $[0,1,1]_{cubic}$ zone axis. The presence of cubic phase inside the lamella explains its lower cobalt content and emphasizes the complex transformation process of cubic perovskite into the $Ba_{1-x}Sr_xCo_{2-y}Fe_yO_{5-\delta}$ structure. It is clearly seen that the diffusion of metal ions play a decisive role in the decomposition process of BSCF. Hence, under the present conditions, BSCF does not exhibit a rigid cationic lattice in that only the oxygen is mobile. This observation supports the interpretation of high creep rates in the intermediate temperature range by Yi et al.[11]

On the basis of the annealing times of the BSCF samples, we assume that the phases reached equilibrium at the conditions under consideration. Figure 12 summarizes the decomposition process of BSCF. The products of BSCF phase transition, cobalt-enriched hexagonal perovskite $Ba_{0.6}Sr_{0.4}CoO_{3-\delta}$, 15R-related $Ba_{1-x}Sr_xCo_{2-y}Fe_yO_{5-\delta}$ complex oxide, and barium, strontium mixed oxide were detected in the TEM study. Because no phases strongly enriched in strontium and iron were found in the annealed BSCF samples, the remaining of strontium and iron in the cubic perovskite may be proposed. Recently, Yáng et al. developed a phase map of a quasi-quaternary Ba−Sr−Co−Fe oxide system at 1273 K, which we adapted in Figure 13.[37] According to this phase map, the end members of the quasi-quaternary system reject to form

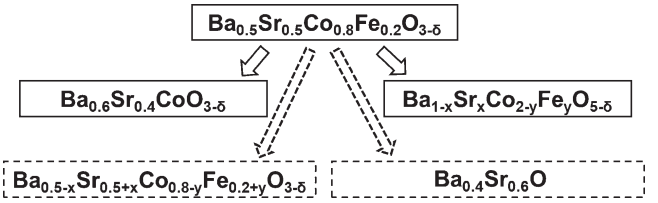

Figure 12. Schematic representation of the BSCF decomposition process.

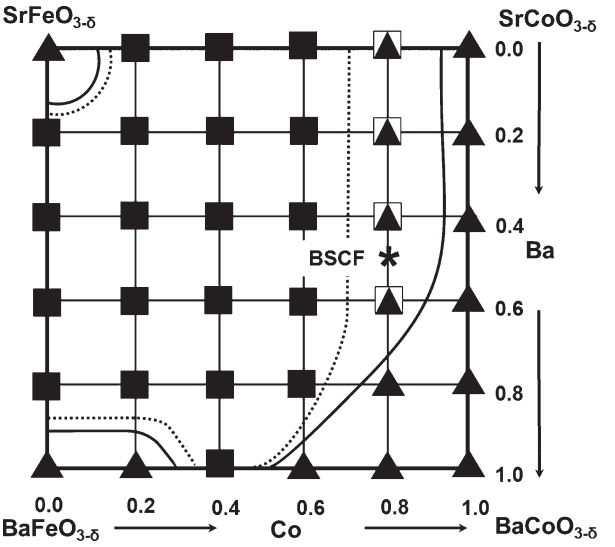

Figure 13. Schematic phase diagram of the quasi-quaternary Ba−Sr−Co−Fe oxide system. Adapted with permission from ref 37. Copyright 2009 International Union of Crystallography. The cubic phases are marked with square symbols; triangle symbols relate to the multiphase compounds. The borderlines each of which is associated with miscibility gap are drawn tentatively as solid lines at 1273 K and as dashed lines at temperatures below 1073 K.

the pure cubic phase. However, the cubic phase prevailed after the mixing of Ba/Sr at the A-site and Co/Fe at the B-site apart from barium- and cobalt-rich compositions. Furthermore, the cubic perovskite can be considered as more stable in the strontium- and iron-rich composition. However, then, it might exhibit poorer transport properties as compared to the initial BSCF composition. Each of the borderlines between the cubic phase field and multiphase compounds in Figure 13 is associated with a miscibility gap, which occurs between phases of dissimilar crystal structures according to the Hume−Rothery rules.[38] The results of the TEM study of BSCF decomposition point out, that the multiphase compound's area to the right of BSCF expands in the direction of strontium- and iron-rich composition in the intermediate temperature range as marked by a dashed line in Figure 13; i.e., the cubic phase field becomes narrowed as temperature decreases from, e.g., 1273 to 1073 K or lower. At temperatures below 1073 K, the parent BSCF phase is located in a miscibility gap between cubic phase and multiphase compounds, which is in good agreement with the report of Mueller et al.[16] Looking again at the Hume−Rothery rules,

(37) Yáng, Z.; Harvey, A. S.; Infortuna, A.; Gauckler, L. J. *J. Appl. Crystallogr.* **2009**, *42*, 153.

(38) Hume-Rothery, W.; Smallman, R. W.; Haworth, C. W. *The Structure of Metals and Alloys*; The Institute of Metals: London, 1969.

we may conclude that effective ionic radii influence the location of the miscibility gap (i.e., the borderlines in Figure 13). In this context, we emphasize that the multiphase formation is initialized by the coupled oxidation and spin-state transition of cobalt cations diminishing their effective ionic radii, which are not tolerated in the cubic perovskite structure. This view is supported by the postulations given by Švarcová et al. and Arnold et al.[13,15,17] In consequence, the cubic BSCF breaks down into the above-mentioned phases involving diffusion of the metal cations.

Conclusions

The current research attests the inherent phase instability of BSCF during heating at intermediate temperatures. We observed that cubic perovskite decomposed into hexagonal perovskite $Ba_{0.6}Sr_{0.4}CoO_{3-\delta}$, lamellar-shaped $Ba_{1-x}Sr_xCo_{2-y}Fe_yO_{5-\delta}$ complex oxide, and $Ba_{0.4}Sr_{0.6}O$. The structure of the previously unknown $Ba_{1-x}Sr_xCo_{2-y}Fe_yO_{5-\delta}$ phase was found to be related to the structure of the 15R hexagonal perovskite polymorph. The several micrometer-long $Ba_{1-x}Sr_xCo_{2-y}Fe_yO_{5-\delta}$ lamellae grew along different directions through the parent cubic phase and can be considered as barriers to oxygen transport due to their shape, low crystal symmetry, and low amount of mobile oxygen vacancies. A change in stoichiometry of the cubic phase is another reason for the degradation of the functional properties. The results of the TEM study support the postulated reason for BSCF decomposition at intermediate temperatures, which has been suggested to be coupled to the valence and spin-state transitions of cobalt ions.

Acknowledgment. The authors greatly acknowledge financial support from the State of Lower Saxony (Germany, NTH bottom-up project, No. 21-71023-25-7/09), from the Deutsche Forschungsgemeinschaft (DFG, Grant FE 928/1-2), and from the European Union under the Framework 6 program by an integrated infrastructure initiative, reference 026019 ESTEEM. K.E. and A.F. appreciate fruitful discussions with Prof. Jürgen Caro.